HHS Public Access

Author manuscript

Nat Methods. Author manuscript; available in PMC 2020 January 15.

Published in final edited form as:

Nat Methods. 2019 August ; 16(8): 771–777. doi:10.1038/s41592-019-0469-9.

High-affinity free ubiquitin sensors for quantifying ubiquitin homeostasis and deubiquitination

Yun-Seok Choi[1], **Sarah A. Bollinger**[1], **Luisa F. Prada**[1], **Francesco Scavone**[1], **Tingting Yao**[1], **Robert E. Cohen**[1,*]

[1]Department of Biochemistry & Molecular Biology, Colorado State University, Fort Collins, Colorado, USA

Abstract

Ubiquitin (Ub) conjugation is an essential post-translational modification that affects nearly all proteins in eukaryotes. The functions and mechanisms of ubiquitination are areas of extensive study, and yet the dynamics and regulation of even free (i.e., unconjugated) Ub are poorly understood. A major impediment has been the lack of simple and robust techniques to quantify Ub levels in cells and to monitor Ub release from conjugates. Here we describe avidity-based fluorescent sensors that address this need. The sensors bind specifically to free Ub, have K_d values down to 60 pM, and, in concert with a newly developed workflow, allow us to distinguish and quantify the pools of free, protein-conjugated, and thioesterified forms of Ub from cell lysates. Alternatively, free Ub in fixed cells can be visualized microscopically by staining with a sensor. Real-time assays using the sensors afford unprecedented flexibility and precision to measure deubiquitination of virtually any (poly)Ub conjugate.

Introduction

In ubiquitination, free Ub (i.e., unconjugated monoUb, or a polyUb chain with a free C-terminus) is activated by formation of a C-terminal thioester first with E1 Ub-activating enzyme and then an E2 Ub-conjugating enzyme before it is transferred to substrates, usually to form an isopeptide bond with a protein lysine ε-amine[1]. Thus, cells contain three classes of Ub: free, thioester-activated, and (iso)peptide conjugated. Because ubiquitination contributes to the regulation of nearly every cellular process, Ub availability must be tightly controlled. Contributions to Ub homeostasis include Ub expression as peptide or protein fusions and as polyubiquitin, processing to generate monoUb, and recycling from Ub–protein conjugates by deubiquitinating enzymes (DUBs)[2]. Perturbations of these processes

*Corresponding author Address correspondence to: Robert E. Cohen, Department of Biochemistry & Molecular Biology, Colorado State University, Fort Collins, CO 80523-1870, bob.cohen@colostate.edu Tel: 970-492-4117.

Author contributions

Y.C. and R.E.C. conceived and designed the ubiquitin sensor reagents, and Y.C. produced the sensors and characterized them in vitro. S.B., T.Y., and R.E.C. conceived of the cell-based studies, which were done by S.B., L.P., and F.S. All authors contributed to writing or commenting on the manuscript.

Competing interests

U.S. patent no. 10,018,634 has been awarded to Colorado State University Research Foundation (R.E.C. and Y.C., inventors) for ubiquitin sensors and assays described in this paper.

can deplete cellular free Ub and cause defects in cell development or neuronal functions[2–9] and inhibit cell proliferation[10,11]. Conversely, transgenic mice overexpressing Ub by just 2 or 3-fold exhibit neurological abnormalities[12].

Although the need to regulate free Ub is well established, studying intracellular Ub pools has been difficult. One approach has been ectopic expression of GFP-tagged Ub[13], but such experiments can be complicated by perturbations to the regulation of endogenous Ub and non-physiological behavior of the tagged Ub. For example, C-terminal tags would prevent Ub activation and conjugation, and N-terminal tags would block assembly of all M1-linked polyUb conjugates. Typically, to quantify endogenous free, conjugated, or total Ub, anti-Ub antibodies in conjunction with ELISA or western blots are used. However, there are major drawbacks. Due to the high structural diversity of polyUb and Ub–protein conjugates[14], binding efficiencies for the different Ub conjugates can vary widely. Moreover, for western blots, dynamic range is inherently very limited and reproducibility can be problematic. Recently, Ub Protein Standard Absolute Quantification (Ub-PSAQ) mass spectrometry (MS) has been described to quantify free and conjugated Ub from cell lysates[15]. However, Ub-PSAQ does not resolve the pool of thioester-activated Ub, and its dependence on sophisticated instrumentation and affinity-isolation steps makes its implementation challenging for most laboratories. Finally, none of the aforementioned approaches allow real-time quantitation of free Ub as it changes, for example, in deubiquitination reactions.

With the dual goals of establishing a simple, reliable method to quantify cellular Ub pools as well as a versatile real-time DUB assay, we embarked on development of sensors for free Ub. Our strategy was to fuse Ub binding domains (UBDs) of known structure that bind to non-overlapping Ub surfaces, and to exploit avidity effects to achieve high affinity and selectivity. To convert the binding proteins into sensors, we attached fluorescent dyes whose intensities changed in response to Ub binding. We then used the sensors to measure free, activated, and conjugated intracellular Ub, to quantify deubiquitination of unlabeled conjugates in real-time, and to identify endogenous free Ub by fluorescence microscopy of fixed cells.

Results

Design and characterization of the sensors

Ub binding proteins were assembled from multiple UBDs linked in tandem. Interdomain peptide linkers were kept short to promote avidity while minimizing the entropic cost of binding. Most UBDs bind through interactions with one of three different Ub surfaces: the hydrophobic patch surrounding residue I44, the C-terminal tail, and the surface around D58 (Fig. 1a, upper panel). Individually, UBDs bind Ub with only modest affinities ($K_d = 10^{-5}$ to 10^{-3} M), but by linking two or three weak-binding UBDs that target distinct surfaces, we predicted that high affinity could be achieved. An early version of an avidity-based binder that we call tIVR employed $IsoT^{Buz}$, $Vps27^{UIM}$, and $Rabex5^{Ruz}$ domains fused with flexible linkers (Fig. 1a, lower left panel; Supplementary Fig. S1). The $IsoT^{Buz}$ domain ($K_d = 3$ μM)[16], which binds primarily to Ub C-terminal residues, conferred selectivity for free Ub, whereas the $Vps27^{UIM}$ ($K_d = 117$ μM)[17] and $Rabex5^{Ruz}$ ($K_d = 12$ μM)[18,19] domains worked synergistically with $IsoT^{Buz}$ to increase overall affinity and specificity.

To measure the affinity between tIVR and free Ub, we first titrated Atto532-Ub(S20C) with tIVR and determined a 0.4 nM K_d for the 1:1 complex (Supplementary Fig. S2a). Then, taking advantage of this high affinity and the 3.5-fold lower fluorescence of Atto532-Ub(S20C) in the complex, we determined tIVR affinities for Ub and other ligands by competition (Fig. 1b). We found that free Ub binds tIVR with a K_d of 19 nM (measured as a K_i; Fig. 1b); the higher affinity of Atto532-Ub(S20C) indicates that the dye promotes the interaction ($\Delta G \sim -0.2$ kcal/mol). The competition assays additionally showed that tIVR has high selectivity against the Ub-like (UbL) protein Nedd8 and Ub derivatives that lack a free C-terminal carboxylate (Fig. 1b). Among the many different UbL proteins in eukaryotes[20], Nedd8 is most similar to Ub in its sequence and tertiary structure, and its C-terminal four amino acids are identical[21]; nonetheless, tIVR has a 3000-fold preference for Ub. A similarly large discrimination was observed against Ub-GB1, a mimic of a Ub–protein conjugate in which the Ub C-terminus is extended by the Protein G B1 domain, and even addition of the small adduct hydrazine to the Ub C-terminus decreased tIVR affinity 150-fold (Fig. 1b).

To provide a direct readout for Ub binding, we explored site-specific labeling with fluorescent dyes (Supplementary Fig. S3). tIVR(C130) modified with Atto532-maleimide showed a 3-fold fluorescence increase upon Ub binding (Supplementary Fig. S2b). By replacing $Vps27^{UIM}$ with the $S5a^{UIM}$ domain and introducing two amino acid substitutions in the $IsoT^{Buz}$ domain (Fig. 1a; Supplementary Fig. S1), we developed a second-generation sensor, tISR, with nearly 10-times the affinity of tIVR for free Ub (Supplementary Fig. S2c,d). Atto532-tISR fluorescence increased 6-fold upon binding Ub and its K_d was 24.3 nM (Fig. 1c; Supplementary Fig. S2b).

A third-generation sensor was developed with the goal of even greater affinity. In tUI, the UIM-RUZ domains of tIVR/tISR were replaced by ubiquilin-1 UBA ($UQ1^{UBA}$), which binds to the Ub hydrophobic patch (K_d = 22 μM)[22,23]. Only 2 amino acids (versus 5 with tIVR or tISR) were needed to connect the $UQ1^{UBA}$ C-terminus with the N-terminus of $IsoT^{Buz}$, which we expected might reduce the entropic cost of complex formation. We conjugated Atto532 to $UQ1^{UBA}$ G573C in tUI (Fig. 1a, lower right panel); titration with Ub revealed a 3-fold fluorescence increase and a remarkably low K_d of 66 ± 16 pM (Fig. 1d,e). We confirmed this by measuring the association and dissociation rate constants for the Atto532-tUI–Ub complex, from which we calculated a K_d of 56.4 ± 1.2 pM (Supplementary Fig. S4). To our knowledge, this high affinity is unprecedented for binding to a single Ub. Atto532-tUI was selective against Ub C-terminal conjugates, preferring free Ub over Ub-GB1 by $>10^6$, and having 120-fold higher affinity for Ub than Nedd8. The greater selectivity against Nedd8 by the tIVR/tISR sensors can be attributed to their Ruz domain, which is absent from tUI. Nonetheless, as described below, tUI's selectivity and high affinity make it the first choice for most *in vitro* applications.

In cells, multiple forms of Ub can have a free C-terminus, and the proximal Ub of free or "unanchored" polyUb chains could be recognized by the Buz domain. Inspection of the sites on Ub used for Ub–Ub linkages (i.e., Ub's seven lysine ε-amines plus the M1 α-amine) showed that they are not occluded when bound by the various UBDs used in the sensors (Fig. 1a). These models are consistent with studies that have shown little or no

discrimination by individual UBA, UIM, or Buz domains for binding Ub in chains with different Ub–Ub linkages[16,22,23]. Accordingly, competition by Ub_2 or Ub_4 representing all 8 Ub–Ub linkages revealed little difference from free monoUb in binding to tIVR (Fig. 1e,f). Based on findings of linkage-independent binding by UBA domains[22,23] and the small tUI footprint modeled onto Ub (Fig. 1a), we anticipate similar linkage-independent binding by tUI to unanchored polyUb.

Another Ub modification that potentially could affect detection by the sensors is phosphorylation. Multiple Ub serine and threonine phosphosites have been identified[24]; as with Ub lysines, most of these do not overlap with the surfaces bound by the sensor UBDs (Fig. 1a). Ub phosphorylation on S65, which has functions in Ub-mediated signaling and mitophagy, has been the most intensively studied phosphoUb species[25–28]. Titration of Atto532-tUI with Ub(pS65) indicated 4-fold weaker binding than with Ub (Fig. 1d,e). Wauer et al. have shown by NMR that Ub(pS65) exists in an equilibrium between two principal conformers[29]. One form (~70%) is essentially like unmodified Ub, whereas in the minor conformer (~30%) movement of the β5 strand retracts the normally-extended C-terminal residues and displaces a key component of the hydrophobic patch. Because interactions with Buz and UBA domains are likely to be disrupted in the minor conformer, the Ub versus Ub(pS65) K_d difference could in part reflect this equilibrium where only a fraction of Ub(pS65) is in the binding-competent conformation.

Real-time deubiquitination assays with label-free substrates

Although desirable, quantitative DUB activity assays rarely employ physiological substrates and have been hampered by the lack of good methods to quantify products. Moreover, real-time monitoring of activity — the preferred approach to high-precision kinetics studies — has been virtually impossible with physiological DUB substrates. For these reasons, artificial substrates such as Ub-(7-amido-4-methylcoumarin) or conjugates (e.g., diUb) modified with fluorophores for FRET-based assays are used[30,31]. Our free Ub sensors make possible less restrictive DUB assays that can employ virtually any Ub conjugate as a substrate. As an example, we used Atto532-tIVR to monitor DUB-catalyzed release of free Ub (or unanchored polyUb) in a continuous fluorometric assay. As a substrate, we used K48-linked Ub_5 conjugated to ovomucoid first domain (OM); the OM moiety also was modified with Lucifer Yellow dye (LY) for detection after SDS-PAGE[32]. For the DUB, we used human OTUB1, which selectively cleaves K48 Ub–Ub linkages[33] and is activated allosterically by certain E2 enzymes[34]. Without OTUB1, Ub_5OM(LY) and Atto532-tIVR showed no fluorescence change, whereas enzyme addition initiated a fluorescence increase corresponding to release of (poly)Ub (Fig. 2); as expected, addition of UbcH5c stimulated the deubiquitination activity[34]. SDS-PAGE confirmed the sensor results (Supplementary Fig. S5). Because OTUB1 cleaves only K48 Ub–Ub linkages, Ub_1-OM(LY) accumulated upon OTUB1 digestion, even with UbcH5c (lane 6, Supplementary Fig. S5a–c). This remaining conjugated Ub could be cleaved by the non-specific DUB Usp2cc (lane 7, Supplementary Fig. S5a–c). The release of free (poly)Ub determined in real-time using the sensor agreed with the amounts calculated by quantifying the LY-labeled gel bands (Supplementary Fig. S5d).

Ub pool quantitation in cell lysates

We next developed methods using the sensors to quantify cellular Ub pools. Our goal was to generate a workflow that would not depend on expensive, time-intensive steps requiring chromatography or mass spectrometry. The general approach, in which sensor (e.g., Atto532-tUI) fluorescence is measured with and without addition of cell lysate or other sample, promised to be simple and direct. The main challenge was to develop conditions to prevent appearance of free Ub due to disassembly of conjugates by endogenous DUBs or from spontaneous hydrolysis of Ub thioesters.

Our strategy was to lyse cells and quickly inactivate endogenous DUBs and other proteases, and then treat each sample in three ways to differentially convert Ub pools to the free-Ub form for measurement with the sensor (Fig. 3a). To measure endogenous free Ub without interference from chemically-labile Ub thioesters, samples were treated with hydrazine to rapidly convert all Ub thioesters into Ub C-terminal hydrazide; Ub-hydrazide is stable and, relative to free Ub, gives a negligible response with the sensor (Fig. 1b–e; Supplementary Fig. S6). Thus, sensor fluorescence of hydrazine-treated samples will measure endogenous free Ub. With a second portion of the sample, β-mercaptoethanol was used to release Ub from thioesters; measurement with the sensor then will report the sum of the endogenous free and thioesterified Ub pools[35]. A third portion was incubated with Usp2cc, a truncated DUB that can deubiquitinate virtually all forms of conjugated Ub[36]; when used in combination with a thiol reducing agent, all forms of Ub are converted to free Ub (Supplementary Fig. S7) and the sensor readout will report the total Ub. By deducting the sum of the thioester-activated and free Ub from the total Ub, we can quantify the conjugated-Ub pool.

We first determined the amounts of free, activated, and conjugated Ub in HeLa cells (Fig. 3); the results are in good agreement with other reports[15,37,38]. The sensor assays then were used with HeLa cells treated with inhibitors of the E1 Ub-activating enzyme or proteasome (Fig. 3b,c). As expected[39], the E1 inhibitor C1 dramatically increased free Ub with a concomitant loss of activated Ub and most Ub–protein conjugates (Fig. 3b). Conversely, proteasome inhibition by bortezomib (BTZ) promoted accumulation of Ub conjugates that reached a maximum at 1 h and then persisted through a 4 h treatment (Fig. 3c; Supplementary Fig. S8). The conjugate increase was accompanied by a modest depletion of activated Ub and a two-fold decrease in free Ub, presumably due to impaired proteasome-dependent recycling of Ub from conjugates. Different from this result, proteasome-inhibited MEF cells exhibited little change in free Ub levels, even though conjugated Ub increased 50%; instead, total Ub increased, likely due to increased expression of Ub genes (Fig. 3c)[40].

Quantitation of endogenous free Ub in fixed cells

Atto532-tUI, with its high affinity and specificity, could be an ideal tool to localize endogenous, intracellular free Ub. Initially, fixed cells were stained directly with Atto532-tUI, but high background fluorescence, possibly from nonspecific binding by the fluorophore, reduced sensitivity (data not shown). Therefore, we used instead hemagglutinin-tagged tUI (HA-tUI) followed by detection with anti-HA antibody. We confirmed the specificity of HA-tUI in control experiments where fixed cells were incubated

with HA-tUI together with excess free Ub. The fluorescence observed in these competition experiments was negligible, suggesting that the staining with HA-tUI is specific for cellular Ub (Supplementary Fig. S9). A diffuse intracellular distribution of free Ub was expected based on its small size (8.6 kDa) and negligible self-association[41]. Staining with HA-tUI was observed throughout the cytoplasm and nuclei of HeLa, U2OS, MEF and RPE1 cells (Fig. 4a). Compared to K48-linked chains and (poly)ubiquitylated proteins, free Ub staining appears evenly distributed throughout the cell (Supplementary Fig. S10). GFP-Ub mutated to prevent its conjugation to other proteins was similarly diffuse when expressed in mammalian cells[13].

Staining with HA-tUI offers an alternative to solution-based assays to monitor changes in free Ub during growth or in response to different stresses. After proteasome inhibition with BTZ for 1 h, HeLa, U2OS, MEF and RPE1 cells showed 1.3 to 1.5-fold less staining with HA-tUI relative to control cells. As expected, E1 inhibition increased the free Ub (2-fold in MEF and RPE cells; 3-fold in HeLa and U2OS cells) (Fig. 4b,c). Although proteasome inhibition decreased free Ub in all four cell lines, the intracellular distributions of free Ub appeared unaffected. For RPE1 cells, ratios of cytoplasmic to nuclear staining were not changed by incubation with BTZ (control cells, 0.85 ± 0.07, n = 5; BTZ, 0.89 ± 0.08, n = 4), whereas increased staining was observed after E1 inhibition and cell-to-cell variability was greater overall (Fig. 4a–c). The changes in staining of HeLa cells are consistent with the in-solution assays, although MEF cell staining indicated ~25% less free Ub after proteasome inhibition than was determined by the in-solution assays (Figs. 3c and 4a–c). Possibly, because hydrazine treatment was not used with the imaged cells, some free Ub detected by staining could have arisen from spontaneous hydrolysis of Ub thioesters, thereby inflating the “free” Ub and confounding direct comparison of the two assays. Staining with tUI also revealed cell cycle-dependent differences in free Ub levels. RPE1 cells undergoing mitosis bound 1.6-fold more HA-tUI than cells in interphase (Fig. 4d). The increase in free Ub may be due, at least in part, to large-scale deubiquitination of H2A histones in mitotic cells[42].

Discussion

Individually, UBDs have only modest affinity for Ub and are typically found together with other binding domains (and sometimes additional UBDs) to promote binding to specific types of (poly)Ub-protein conjugates. From genetic fusions of multiple UBDs, we have engineered new proteins with specificity and high affinity for monomeric free Ub. Our basic strategy was to use the Buz domain to direct binding to Ub with an unconjugated C-terminus, and to increase affinity with one or two additional UBDs that interact with Ub on non-overlapping surfaces. Critical to this design strategy was maximizing avidity. This was achieved by having multiple UBDs bind simultaneously while minimizing the entropy lost upon complex formation through careful selection of peptides linking the UBDs. Avid binding can boost affinity by combining the contributions of individual binding domains in a complex assembled from a multivalent ligand and a corresponding multivalent binder. The Gibbs free energy for binding overall (ΔG_{total}) can be approximated as the sum of the individual binding domain (BD) interaction free energies (ΔG_{BD1}, ΔG_{BD2}, etc.) plus the unfavorable free energy due to reduction in entropy (predominantly, losses in translational and rotational entropy) from having all the binding domains linked together (ΔG_S)[43]:

$$\Delta G_{total} = \Delta G_{BD1} + \Delta G_{BD2} \cdot \cdot \cdot \cdot + \Delta G_{BDn} + \Delta G_S \quad (1)$$

To achieve "perfect" avid binding and maximize affinity, ΔG_S should be close to zero. For Ub binding by a tandem-UBD (tUBD) protein such as tIVR:

$$\Delta G_{tUBD} = \Delta G_{UBD1} + \Delta G_{UBD2} + \Delta G_{UBD3} + \Delta G_S \quad (2)$$

ΔG_{UBD} can be calculated for each UBD based on the K_d values reported for Ub binding by the individual IsoT^{Buz}, Vps27^{UIM}, and Rabex5^{Ruz} domains (i.e., −7.53, −5.25, and −6.62 kcal·mol^{-1}, respectively); similarly, ΔG_{tIVR} = −10.52 kcal·mol^{-1} can be calculated from the tIVR–Ub K_d of 19.3 nM (Fig. 1e). Thus, although avidity promotes tight binding by tIVR, it's at the cost of ΔG_S, which is (−10.52) – (−19.40) = 8.88 kcal·mol^{-1}. This substantial penalty reduced tIVR affinity by >10^6 from a theoretical K_d of 5.9 × 10^{-15} M.

Remarkably, tUI's affinity for Ub (K_i = 194 pM; Supplementary Fig. S11) is only 3-times weaker than what would be predicted for *perfect* avid binding by the combination of the UQ1^{UBA} (K_d = 22 μM)[22,23] and Buz (K_d = 3 μM)[16] domains. Contributing to this highly efficient avidity effect is that tUI has only one linker peptide (versus two in tIVR), and it is very short (Supplementary Fig. S1). Thus, a likely route to increase affinity for tIVR or tISR is further optimization of the interdomain linkers. On the other hand, a large increase in tUI's affinity would have to come from tighter-binding versions of one or both UBDs, as the linker already is nearly optimal.

There are several ways in which our free Ub sensors could be improved. Affinity might be increased, as noted above, with either modified linkers or alternative UBDs. Our designs have utilized only a few of more than 20 types of UBDs[44,45]; moreover, other Ub binding proteins such as catalytically-inactive DUBs might be used as components of tUBD-type fusion constructs[46]. Particularly intriguing is the prospect of tailoring recognition by incorporation of a UBD that would select either for or against specific modifications on the Ub. For example, although tIVR binds equally well to free polyUb chains of different Ub–Ub linkage types (Fig. 1f), modified Ruz or UIM domains could be developed in which steric clash prevents binding to Ub conjugated at particular lysine(s). Similarly, UBD (or linker) modifications might add selectivity for phosphoUb derivatives. Finally, alternative fluorophores and attachment sites can be explored to improve sensor sensitivity and dynamic range.

The free Ub binders and the fluorescent sensors developed from them provide new tools to capture, deplete, quantify, or visualize free Ub *in vitro* and in cells. Multiple DUBs have been implicated in human disease[47], but DUB inhibitor screens generally have been limited to non-physiological substrates. The real-time sensor-based assays will make possible high-throughput screens with virtually any Ub conjugate as the substrate. Other examples include neurological disorders where Ub homeostasis is disrupted and accompanied by Ub-containing aggregates or a general depletion of free Ub. Staining by tUI offers a new

approach to examine neurons at the single-cell level to study the effects of genetic or environmental perturbations on Ub homeostasis and intracellular distribution. Extracellular free Ub is of interest as well, as it has been suggested as a biomarker for trauma and disease[48]; here also, the sensors can replace the less specific antibody-based assays typically used.

Online Methods

Materials and protein preparation

tIVR, tISR, tUI, Ub-GB1, and UbcH5c were cloned into pET28a and transformed into BL21-CodonPlus (DE3) E. coli cells for protein expression. Expression was induced by the addition of 0.4 mM IPTG to cells grown at 37 °C to OD_{660nm} = 0.6–0.8, and then growth was continued at 25 °C for 8 h. The cells were harvested by centrifugation at 3,200 x *g*, resuspended in ice-cold Buffer A (20 mM sodium phosphate, pH 7.4, 500 mM NaCl, 10 mM imidazole, and 10 mM β-mercaptoethanol), and lysed by sonication; the lysates were clarified by centrifugation for 30 min at 4 °C at 20,199 x *g*. A Histrap HP column (GE Healthcare, 17–5248-02) was used to purify the proteins from the lysates. Samples were applied to the column equilibrated with Buffer A, and after washing with 20 column volumes, bound proteins were eluted with a linear gradient to 500 mM imidazole in Buffer A. The proteins were further purified by gel filtration through a Superdex 75 column (GE Healthcare, 29–1487-21) eluted with pH 7.4 PBS and 1 mM DTT or 1 mM TCEP. Purity was confirmed by SDS-PAGE. Ub[49], Nedd8[50], Usp2cc[36], and Ub_5-OM(LY)[32] were prepared as described. OTUB1 was a gift from C. Wolberger (Johns Hopkins University). K6, K11, K27, K29, K33, K48, and K63-linked Ub_2 chains were purchased from UbiQ Bio (Amsterdam), Ub(pS65) was from BostonBiochem (Cambridge, MA), and M1-linked Ub_4 was prepared as described[51].

Synthesis of Ub-hydrazide

Ub (1.5 mM) was incubated with 10 mM ATP, 10 mM $MgCl_2$, 100 mM sodium 2-mercaptoethanesulfonate (MESNA; Fluka), and 100 nM mouse E1 in 20 mM HEPES (pH 8.0) for 3 h at 37 °C to form Ub-MESNA thioester (confirmed by mass spectrometry; see Supplementary Fig. S6b). The Ub-MESNA then was incubated in 300 mM aqueous hydrazine for 30 min at 37 °C to form Ub-hydrazide. The reaction product was diluted 25-fold with 50 mM ammonium acetate, adjusted to pH 4.5 (Buffer B), and purified by cation-exchange chromatography on a Mono S column (GE Healthcare, 17–0547-01). The column was washed with 20 volumes of Buffer B and eluted with a linear gradient of 0 – 1 M NaCl in the same buffer. The purified Ub-hydrazide was confirmed by mass spectrometry (Supplementary Fig. S6b).

Fluorophore labeling

Sensor proteins were labeled at cysteine with fluorophore-maleimide dyes from ATTO-TEC GmbH (Atto dyes; see Supplementary Fig. S3), Molecular Probes (Alexa Fluor 488), or Anaspec (fluorescein). Fluorophore-maleimide dyes (1.5 to 5-fold molar excess) were incubated with 50 μM sensor in 50 mM HEPES, pH 7.4, 100 mM NaCl for 2 h at 25 °C. Excess dyes were quenched by incubation with 10 mM β-mercaptoethanol for 10 min at

25 °C. To remove excess dyes, the reaction product was bound to Ni-NTA resin (Thermo Fisher) equilibrated with Buffer A, the resin was washed 5 times with the Histrap binding buffer, and sensor proteins were eluted with Histrap elution buffer. Labeling was confirmed by SDS-PAGE and then scanning the gel for fluorescence using a Typhoon FLA 9500 (GE Healthcare Life Sciences). Degree of labeling (DOL) and concentrations of the labeled proteins were calculated by the equations below.

$$\mathrm{DOL} = \frac{A_m \times \varepsilon_{prot}}{\left(A_{280} - A_m \times CF_{280}\right) \times \varepsilon_m} \qquad CF_{280} = \frac{\varepsilon_{280}}{\varepsilon_m}$$

$$\text{Protein concentration (M)} = \frac{\left(A_{280} - \left(A_m \times CF_{280}\right)\right)}{\varepsilon_{prot}}$$

In the equations, A_m represents the absorbance at the dye absorption maximum, A_{280} is absorbance at 280 nm of the labeled protein, ε_{prot} is the extinction coefficients at 280 nm of the protein, ε_{280} is the extinction coefficient at 280 nm of the dye alone, ε_m is the extinction coefficient at the absorption maximum of the dye, and CF_{280} is the correction factor at 280 nm.

Binding assays

All binding assays were done in PBS buffer, pH 7.4, supplemented with 0.05% Brij35 and either 0.2 mg/ml ovalbumin or GB1 protein, and either 1 mM DTT or 1 mM TCEP. A FluoroMax-4 spectrofluorimeter (HORIBA Scientific) was used to measure fluorescence intensity in the binding assays. K_d and K_i values were calculated by fitting with a single-site binding model[52] using Prism 6 (GraphPad Software). Because of its high affinity for Ub, only 10 pM Atto532-tUI was used in the binding assays to keep its concentration below the K_d. To improve detection of the fluorescence from this low concentration of Atto532-tUI, we increased the assay volume to 2.7 ml. The stock Ub titrated into the solution was ≤ 1.5% of the total volume.

Stopped flow kinetics

To determine the k_{off} and k_{on} rates of Atto532-tUI with free Ub, rapid kinetics were monitored by fluorescence using a MOS-500 spectrometer equipped with a SFM-4000 mixer (Bio-Logic Science Instruments) maintained at 25 °C. The excitation wavelength was set to 530 nm with a 5 nm bandwidth, and the fluorescence emission was detected with a 540–620 nm bandpass filter.

Real-time DUB assays

A Fluoromax-4 spectrofluorimeter (HORIBA Scientific) was used to monitor fluorescence of samples (45 μL) in ultramicro quartz cuvettes (Hellma) at 25 °C. The buffer was PBS, pH 7.4, with 0.05% Brij35, 0.2 mg/ml ovalbumin, and 1 mM DTT. A standard curve was generated to convert change in sensor fluorescence to the corresponding free Ub concentrations; e.g., 2 nM Atto532-tIVR was titrated with 2, 3, 6, 10, 18, and 32 nM Ub,

and the binding curve was fit as described above. Fluorescent intensities from real-time DUB assays then were converted to free Ub concentrations using the fitted binding equation. For deubiquitination of Ub_5-OM(LY), results were confirmed by SDS-PAGE of samples from the reaction mixtures and fluorescence imaging of the gel with a Typhoon FLA 9500 laser scanner (GE Healthcare Life Sciences).

In-solution Ub pool assays

Sample preparation—Cells were lysed in 100 mM MOPS, pH 6.0, 8 M urea, 20 mM NEM, and EDTA-free Complete protease inhibitors (Roche) by sonication and then centrifuged at 15,800 x *g*. Total protein in the clarified extract was measured using the bicinchoninic acid (BCA) assay before being divided into three fractions for treatment with Usp2cc, β-mercaptoethanol, or hydrazine. The fraction to be treated with Usp2cc was diluted with digestion buffer (25 mM HEPES, pH 7.5, 140 mM NaCl, and 10 mM DTT) to reduce the urea to less than 2 M; to this, Usp2cc was added at a 1:10 (Usp2cc:total protein) ratio and incubated at 37 °C for 1 h. To another fraction of the extract, 100 mM CHES, pH 9, containing 150 mM β-mercaptoethanol was added and incubated at 37 °C for 1 h. The third fraction was incubated at 37 °C for 1 h with freshly-made 200 mM hydrazine-HCl, pH 8.5. These samples were then diluted using PBS and 0.2 mg/ml ovalbumin to insure that [Ub] was within the linear range of the assay (e.g., with Atto532-tUI, from 2–60 nM). Dilution was also performed to reduce the concentrations of urea (<0.2 M), β-mercaptoethanol (<20 mM), hydrazine (<20 mM), which otherwise can interfere with binding by the sensor.

Negative control for the in-solution Ub pool assays—Samples were depleted of free Ub by incubation with excess E1, ATP, and C1 (an adenosine sulfamate E1 inhibitor). E1 efficiently converts free Ub to a Ub-C1 C-terminal adduct[39], which we expected would prevent binding to the sensor. Clarified cell lysate containing ~1.5 μM free Ub was incubated with 2 μM recombinant human E1 enzyme, 50 μM C1, 10 mM $MgCl_2$, and 250 μM ATP for 1 h at room temperature before addition of Atto532-tUI (see below) and fluorescence was measured. Relative to the untreated lysate, 95% of the Atto532-tUI fluorescence increase from addition of lysate was lost. Thus non-specific binding accounts for no more than 5% of the sensor readout in the assays.

In-solution high-throughput assay to measure free Ub—Microplates (384-well SensoPlate Plus, Greiner Bio-One 781856) were used to measure free Ub concentrations of unknown samples in a high-throughput format. The plates were passivated by sequential treatment with 1% Hellmanex detergent, 1 M KOH, and then 2% 1,7-dichloro-octamethyltetrasiloxane (Sigma-Aldrich) diluted in heptane, where each step was a 30 min soak followed by extensive washes with distilled water and finally air-drying. Typically, 24 μl of a master mix containing 50 nM Atto532-tUI and assay buffer (200 mM sodium phosphate, pH 7.5, 50 mM NaCl, 2 mM DTT, 0.05% Brij35, and 0.2 mg/ml ovalbumin) was added to wells of the passivated 384-well plate. Then, to one set of wells, Ub standards were added and the remaining wells were used for samples (6 μl). Fluorescence intensities were quantified with a Typhoon FLA 9500 laser scanner (GE Healthcare). The Ub concentrations

of unknown samples were determined by interpolating the fluorescent signals on standard curves generated by titration with a standard of free Ub.

Western blotting

Cells were lysed and prepared as for the in-solution pool assays. Lysate samples were separated by SDS-PAGE followed by western blotting onto nitrocellulose (0.2 μm, Bio-Rad). After blocking in PBS with 0.05% Tween-20 and 5% nonfat dry milk, membranes were incubated with anti-Ub (clone P4G7, Santa Cruz Biotechnology, 1:1000 dilution) and anti-alpha tubulin (clone DMIA, Abcam, 1:50,000 dilution) mouse monoclonal antibodies overnight at 4 °C, washed with blocking buffer, and then incubated with IRDy® 680CW-conjugated goat anti-mouse (1:10,000, LI-COR) for 1 h. Imaging was done with a LI-COR Odyssey.

Sample preparation for microscopy

HeLa (ATCC), U2OS, and MEF cells were cultured in DMEM (Gibco) supplemented with 10% (v/v) FBS and 100 U/mL penicillin and 100 ug/mL streptomycin (Hyclone). RPE1 (ATCC) cells were cultured in DMEM/Ham's F-12, 50/50 mix (Corning). The U2OS and MEF cells used were previously described[53]. Cells were incubated for 1 hour with 1 μM bortezomib (Ubiquitin-Proteasome Biotechnologies), 10 μM E1 inhibitor (Compound 1; provided by Takeda Oncology, Cambridge, MA) or vehicle alone (0.1% DMSO). Each experiment was performed a minimum of two times.

We fixed cells at <80% confluence with 4% paraformaldehyde in PBS for 30 min at 37 °C, permeabilized them with 0.1% Triton X-100 for 10 min at room temperature and blocked for 1 hour with 5% BSA and 0.5% Tween 20 in PBS. Cells were stained for free Ub with 100 nM tUI-HA diluted in blocking solution for 30 min at room temperature. As a negative control, the sensor was pre-incubated for 5 min at room temperature with 100 μM Ub in blocking solution before addition to the samples. Next, cells were incubated overnight at 4 °C with anti-HA antibody (Sigma-Aldrich clone HA-7 or Bethyl Laboratories A190–108A; 1:1000 dilution), stained with Alexa Fluor 568-conjugated goat anti-mouse IgG (Thermo Fisher; 1:500 dilution), and mounted on slides using ProLong Diamond Antifade medium (Thermo Fisher). Some coverslips were also stained with anti-Ub (clone FK2, Enzo Life Sciences; 1:1,000 dilution) or anti-K48Ub (clone Apu2, Millipore; 1:200 dilution) primary antibodies and, subsequently, with Alexa Fluor 568-conjugated goat anti-mouse and Alexa Fluor 488-conjugated goat anti-rabbit (Thermo Fisher; 1:400 dilution) secondary antibodies. The HCS CellMask dye (Thermo Fisher) was added to the cells for 0.5 h as a marker of cell boundaries for high-content fluorescence intensity-based measurements.

Microscopy and image analysis

Cells were imaged using a Zeiss LSM 880 confocal microscope with C-Apochromat 40X/1.20 W or Plan-Apochromat 63x/1.40 Oil DIC M27 objectives. Z-stack images were acquired with ZEN Black software (Version 14.0.9.201) at 0.746 μm intervals. ImageJ 1.51h (NIH) was used to perform maximum intensity projections of z-sections and to calculate cell mean fluorescence intensity values; cell contours were drawn using HCS CellMask dye as a reference, and nuclei were identified with DAPI stain. Autofluorescence intensities recorded

from unstained cells were subtracted from the tUI-fluorescence. Three-dimensional reconstructions of RPE-1 cells were obtained with Imaris software (version 9.1.1, Bitplane AG) from serial z-sections acquired at 0.242 μm increments. The Imaris surface creation tool was used to generate volume renderings and to quantify tUI fluorescence intensities in interphase and mitotic cells.

Statistical Analysis

Statistical calculations were performed with GraphPad Prism software and are described in the relevant figure legends. *P* values less than 0.05 were considered significant.

Material availability

Plasmids for bacterial expression of tUI, tUI-HA, tIVR, and tISR are available from Addgene.org (Addgene ID 122661, 122662, 122663, and 122664, respectively).

Reporting Summary

Further information on research design is available in the Nature Research Reporting Summary linked to this article.

Data Availability

The data that support the findings of this paper are available from the corresponding author upon reasonable request.

Supplementary Material

Refer to Web version on PubMed Central for supplementary material.

Acknowledgements

We thank A. Ma (University of California, San Francisco) for MEF cells, C. Wolberger (Johns Hopkins University) for OTUB1 protein, and B. Brasher (Boston Biochem, Cambridge, MA) for phosphoubiquitin. We also thank O. Peersen for assistance with the rapid-kinetics experiments and use of the Bio-Logic stopped-flow spectrofluorometer, and R. Handa for use of the Imaris image analysis software. This research was supported by NIH-NIGMS grant R01 GM115997 (to R.E.C.) and NIH-NIEHS grant R21 ES029150 (to R.E.C. and T.Y.).

References

1. Komander D & Rape M The ubiquitin code. Annu Rev Biochem 81, 203–229, doi:10.1146/annurev-biochem-060310-170328 (2012). [PubMed: 22524316]
2. Park CW & Ryu KY Cellular ubiquitin pool dynamics and homeostasis. BMB Rep 47, 475–482 (2014). [PubMed: 24924398]
3. Ryu KY, Garza JC, Lu XY, Barsh GS & Kopito RR Hypothalamic neurodegeneration and adult-onset obesity in mice lacking the Ubb polyubiquitin gene. Proc Natl Acad Sci U S A 105, 4016–4021, doi:10.1073/pnas.0800096105 (2008). [PubMed: 18299572]
4. Ryu KY et al. The mouse polyubiquitin gene UbC is essential for fetal liver development, cell-cycle progression and stress tolerance. EMBO J 26, 2693–2706, doi:10.1038/sj.emboj.7601722 (2007). [PubMed: 17491588]
5. Ryu KY et al. The mouse polyubiquitin gene Ubb is essential for meiotic progression. Mol Cell Biol 28, 1136–1146, doi:10.1128/MCB.01566-07 (2008). [PubMed: 18070917]

6. Kimura Y et al. An inhibitor of a deubiquitinating enzyme regulates ubiquitin homeostasis. Cell 137, 549–559, doi:10.1016/j.cell.2009.02.028 (2009). [PubMed: 19410548]
7. Wang CH et al. USP5/Leon deubiquitinase confines postsynaptic growth by maintaining ubiquitin homeostasis through Ubiquilin. Elife 6, doi:10.7554/eLife.26886 (2017).
8. Crimmins S et al. Transgenic rescue of ataxia mice with neuronal-specific expression of ubiquitin-specific protease 14. J Neurosci 26, 11423–11431, doi:10.1523/JNEUROSCI.3600-06.2006 (2006). [PubMed: 17079671]
9. Chen PC et al. The proteasome-associated deubiquitinating enzyme Usp14 is essential for the maintenance of synaptic ubiquitin levels and the development of neuromuscular junctions. J Neurosci 29, 10909–10919, doi:10.1523/JNEUROSCI.2635-09.2009 (2009). [PubMed: 19726649]
10. Oh C, Park S, Lee EK & Yoo YJ Downregulation of ubiquitin level via knockdown of polyubiquitin gene Ubb as potential cancer therapeutic intervention. Sci Rep 3, 2623, doi:10.1038/srep02623 (2013). [PubMed: 24022007]
11. Kedves AT et al. Recurrent ubiquitin B silencing in gynecological cancers establishes dependence on ubiquitin C. J Clin Invest 127, 4554–4568, doi:10.1172/JCI92914 (2017). [PubMed: 29130934]
12. Hallengren J, Chen PC & Wilson SM Neuronal ubiquitin homeostasis. Cell Biochem Biophys 67, 67–73, doi:10.1007/s12013-013-9634-4 (2013). [PubMed: 23686613]
13. Dantuma NP, Groothuis TA, Salomons FA & Neefjes J A dynamic ubiquitin equilibrium couples proteasomal activity to chromatin remodeling. J Cell Biol 173, 19–26, doi:10.1083/jcb.200510071 (2006). [PubMed: 16606690]
14. Yau R & Rape M The increasing complexity of the ubiquitin code. Nat Cell Biol 18, 579–586, doi:10.1038/ncb3358 (2016). [PubMed: 27230526]
15. Kaiser SE et al. Protein standard absolute quantification (PSAQ) method for the measurement of cellular ubiquitin pools. Nat Methods 8, 691–696, doi:10.1038/nmeth.1649 (2011). [PubMed: 21743460]
16. Reyes-Turcu FE et al. The ubiquitin binding domain ZnF UBP recognizes the C-terminal diglycine motif of unanchored ubiquitin. Cell 124, 1197–1208, doi:10.1016/j.cell.2006.02.038 (2006). [PubMed: 16564012]
17. Swanson KA, Kang RS, Stamenova SD, Hicke L & Radhakrishnan I Solution structure of Vps27 UIM-ubiquitin complex important for endosomal sorting and receptor downregulation. EMBO J 22, 4597–4606, doi:10.1093/emboj/cdg471 (2003). [PubMed: 12970172]
18. Lee S et al. Structural basis for ubiquitin recognition and autoubiquitination by Rabex-5. Nat Struct Mol Biol 13, 264–271, doi:10.1038/nsmb1064 (2006). [PubMed: 16462746]
19. Penengo L et al. Crystal structure of the ubiquitin binding domains of rabex-5 reveals two modes of interaction with ubiquitin. Cell 124, 1183–1195, doi:10.1016/j.cell.2006.02.020 (2006). [PubMed: 16499958]
20. Maupin-Furlow JA Ubiquitin-like proteins and their roles in archaea. Trends Microbiol 21, 31–38, doi:10.1016/j.tim.2012.09.006 (2013). [PubMed: 23140889]
21. Choi YS, Jeon YH, Ryu KS & Cheong C 60th residues of ubiquitin and Nedd8 are located out of E2-binding surfaces, but are important for K48 ubiquitin-linkage. FEBS Lett 583, 3323–3328, doi:10.1016/j.febslet.2009.09.034 (2009). [PubMed: 19782077]
22. Zhang D, Raasi S & Fushman D Affinity makes the difference: nonselective interaction of the UBA domain of Ubiquilin-1 with monomeric ubiquitin and polyubiquitin chains. J Mol Biol 377, 162–180, doi:10.1016/j.jmb.2007.12.029 (2008). [PubMed: 18241885]
23. Sokratous K et al. Probing affinity and ubiquitin linkage selectivity of ubiquitin-binding domains using mass spectrometry. J Am Chem Soc 134, 6416–6424, doi:10.1021/ja300749d (2012). [PubMed: 22428841]
24. Swaney DL, Rodriguez-Mias RA & Villen J Phosphorylation of ubiquitin at Ser65 affects its polymerization, targets, and proteome-wide turnover. EMBO Rep 16, 1131–1144, doi:10.15252/embr.201540298 (2015). [PubMed: 26142280]
25. Kane LA et al. PINK1 phosphorylates ubiquitin to activate Parkin E3 ubiquitin ligase activity. J Cell Biol 205, 143–153, doi:10.1083/jcb.201402104 (2014). [PubMed: 24751536]

26. Ordureau A et al. Defining roles of PARKIN and ubiquitin phosphorylation by PINK1 in mitochondrial quality control using a ubiquitin replacement strategy. Proc Natl Acad Sci U S A 112, 6637–6642, doi:10.1073/pnas.1506593112 (2015). [PubMed: 25969509]
27. Koyano F et al. Ubiquitin is phosphorylated by PINK1 to activate parkin. Nature 510, 162–166, doi:10.1038/nature13392 (2014). [PubMed: 24784582]
28. Harper JW, Ordureau A & Heo JM Building and decoding ubiquitin chains for mitophagy. Nat Rev Mol Cell Biol 19, 93–108, doi:10.1038/nrm.2017.129 (2018). [PubMed: 29358684]
29. Wauer T et al. Ubiquitin Ser65 phosphorylation affects ubiquitin structure, chain assembly and hydrolysis. EMBO J 34, 307–325, doi:10.15252/embj.201489847 (2015). [PubMed: 25527291]
30. Dang LC, Melandri FD & Stein RL Kinetic and mechanistic studies on the hydrolysis of ubiquitin C-terminal 7-amido-4-methylcoumarin by deubiquitinating enzymes. Biochemistry 37, 1868–1879, doi:10.1021/bi9723360 (1998). [PubMed: 9485312]
31. Geurink PP et al. Development of Diubiquitin-Based FRET Probes To Quantify Ubiquitin Linkage Specificity of Deubiquitinating Enzymes. Chembiochem 17, 816–820, doi:10.1002/cbic.201600017 (2016). [PubMed: 26996281]
32. Yao T & Cohen RE Ubiquitin-ovomucoid fusion proteins as model substrates for monitoring degradation and deubiquitination by proteasomes. Methods Enzymol 398, 522–540, doi:10.1016/S0076-6879(05)98043-9 (2005). [PubMed: 16275356]
33. Wang T et al. Evidence for bidentate substrate binding as the basis for the K48 linkage specificity of otubain 1. J Mol Biol 386, 1011–1023, doi:10.1016/j.jmb.2008.12.085 (2009). [PubMed: 19211026]
34. Wiener R et al. E2 ubiquitin-conjugating enzymes regulate the deubiquitinating activity of OTUB1. Nat Struct Mol Biol 20, 1033–1039, doi:10.1038/nsmb.2655 (2013). [PubMed: 23955022]
35. Gates ZP, Stephan JR, Lee DJ & Kent SB Rapid formal hydrolysis of peptide-alphathioesters. Chem Commun (Camb) 49, 786–788, doi:10.1039/c2cc38229f (2013). [PubMed: 23233036]
36. Shahnawaz M, Thapa A & Park IS Stable activity of a deubiquitylating enzyme (Usp2-cc) in the presence of high concentrations of urea and its application to purify aggregation-prone peptides. Biochem Biophys Res Commun 359, 801–805, doi:10.1016/j.bbrc.2007.05.186 (2007). [PubMed: 17560941]
37. Kim W et al. Systematic and quantitative assessment of the ubiquitin-modified proteome. Mol Cell 44, 325–340, doi:10.1016/j.molcel.2011.08.025 (2011). [PubMed: 21906983]
38. Yang X et al. Absolute quantification of E1, ubiquitin-like proteins and Nedd8-MLN4924 adduct by mass spectrometry. Cell Biochem Biophys 67, 139–147, doi:10.1007/s12013-013-9625-5 (2013). [PubMed: 23754621]
39. Chen JJ et al. Mechanistic studies of substrate-assisted inhibition of ubiquitin-activating enzyme by adenosine sulfamate analogues. J Biol Chem 286, 40867–40877, doi:10.1074/jbc.M111.279984 (2011). [PubMed: 21969368]
40. Bianchi M et al. Dynamic transcription of ubiquitin genes under basal and stressful conditions and new insights into the multiple UBC transcript variants. Gene 573, 100–109, doi:10.1016/j.gene.2015.07.030 (2015). [PubMed: 26172870]
41. Liu Z et al. Noncovalent dimerization of ubiquitin. Angew Chem Int Ed Engl 51, 469–472, doi:10.1002/anie.201106190 (2012). [PubMed: 22109817]
42. Joo HY et al. Regulation of cell cycle progression and gene expression by H2A deubiquitination. Nature 449, 1068–1072, doi:10.1038/nature06256 (2007). [PubMed: 17914355]
43. Jencks WP On the attribution and additivity of binding energies. Proc Natl Acad Sci U S A 78, 4046–4050 (1981). [PubMed: 16593049]
44. Scott D, Oldham NJ, Strachan J, Searle MS & Layfield R Ubiquitin-binding domains: mechanisms of ubiquitin recognition and use as tools to investigate ubiquitin-modified proteomes. Proteomics 15, 844–861, doi:10.1002/pmic.201400341 (2015). [PubMed: 25327553]
45. Hicke L, Schubert HL & Hill CP Ubiquitin-binding domains. Nat Rev Mol Cell Biol 6, 610–621, doi:10.1038/nrm1701 (2005). [PubMed: 16064137]
46. Morrow ME et al. Active site alanine mutations convert deubiquitinases into high-affinity ubiquitin-binding proteins. EMBO Rep 19, doi:10.15252/embr.201745680 (2018).

47. Harrigan JA, Jacq X, Martin NM & Jackson SP Deubiquitylating enzymes and drug discovery: emerging opportunities. Nat Rev Drug Discov 17, 57–78, doi:10.1038/nrd.2017.152 (2018). [PubMed: 28959952]

48. Majetschak M Extracellular ubiquitin: immune modulator and endogenous opponent of damage-associated molecular pattern molecules. J Leukoc Biol 89, 205–219, doi:10.1189/jlb.0510316 (2011). [PubMed: 20689098]

Methods-only References

49. Raasi S & Pickart CM Ubiquitin chain synthesis. Methods Mol Biol 301, 47–55, doi: 10.1385/1-59259-895-1:047 (2005). [PubMed: 15917625]

50. Whitby FG, Xia G, Pickart CM & Hill CP Crystal structure of the human ubiquitin-like protein NEDD8 and interactions with ubiquitin pathway enzymes. J Biol Chem 273, 34983–34991 (1998). [PubMed: 9857030]

51. Wilkinson KD et al. Metabolism of the polyubiquitin degradation signal: structure, mechanism, and role of isopeptidase T. Biochemistry 34, 14535–14546 (1995). [PubMed: 7578059]

52. Wilkinson KD Quantitative analysis of protein-protein interactions. Methods Mol Biol 261, 15–32, doi:10.1385/1-59259-762-9:015 (2004). [PubMed: 15064447]

53. Pasupala N et al. OTUB1 non-catalytically stabilizes the E2 ubiquitin-conjugating enzyme UBE2E1 by preventing its autoubiquitination. J Biol Chem 293, 18285–18295, doi:10.1074/jbc.RA118.004677 (2018). [PubMed: 30282802]

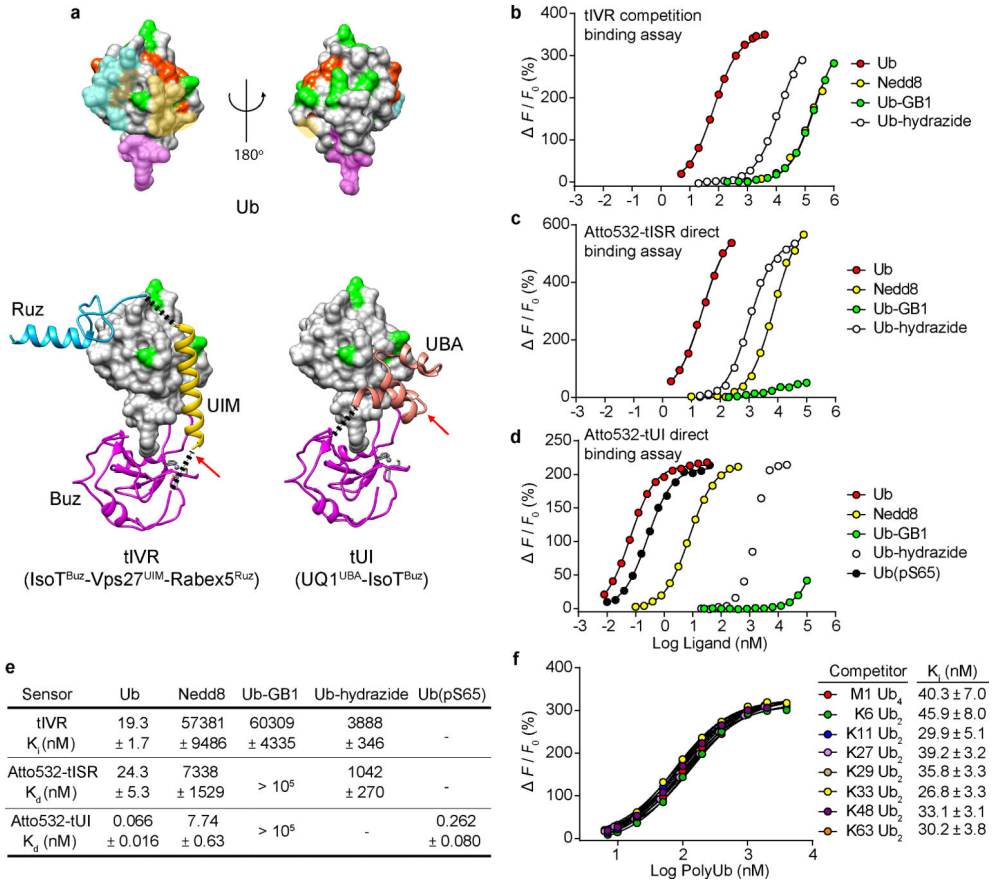

Sensor	Ub	Nedd8	Ub-GB1	Ub-hydrazide	Ub(pS65)
tIVR K_i (nM)	19.3 ± 1.7	57381 ± 9486	60309 ± 4335	3888 ± 346	-
Atto532-tISR K_d (nM)	24.3 ± 5.3	7338 ± 1529	> 10^5	1042 ± 270	-
Atto532-tUI K_d (nM)	0.066 ± 0.016	7.74 ± 0.63	> 10^5	-	0.262 ± 0.080

Fig. 1. Sensor design and characterization.

a, Ub (upper panel) has distinct surfaces recognized by three classes of UBDs. Ub and UBDs are shown in surface and ribbon representations, respectively. For Ub (upper models; from PDB 2G45), surfaces where Buz, UIM or UBA, and Ruz domains bind are in magenta, yellow, and cyan, respectively (PDB 2G45, 2FIF, 1Q0W, and 2JY6). Lysine and M1 sidechains (green) and phosphorylation sites (orange) are highlighted. Ub complexes with tIVR (lower left) and tUI (lower right) were modeled from composites of individual UBD-Ub complex structures. The black dotted lines indicate linkers installed to connect UBDs, and red arrows show sites of fluorophore attachment. **b,** tIVR affinities for Ub and UbL derivatives were measured by competition with 1 nM Atto532-Ub(S20C) in the presence of 6 nM tIVR. ΔF is the fluorescence intensity change of Atto532-Ub(S20C) upon addition of competitor and F_0 is the fluorescence without competitor. Fluorescence intensity changes of **(c)** Atto532-tISR or **(d)** Atto532-tUI were measured by direct titrations with the Ub or UbL derivatives indicated and fit with a 1:1 binding model as described in Methods. The points shown are averages from duplicate samples. **e,** Affinities (K_d or K_i) of the three sensors determined for the indicated Ub and UbL ligands. **f,** Effects of Ub–Ub linkage type were assessed from competition binding assays with 0.8 nM Atto532-Ub(S20C) and 6.0 nM tIVR titrated with 7 to 4000 nM of the indicated polyUb ligands. Errors listed are standard deviations from the fits. Because in **d** the binding curve with Ub-hydrazide might reflect trace contamination by free Ub, a K_d value is not shown.

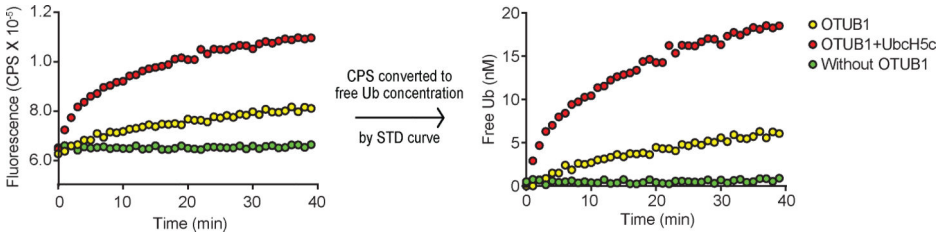

Fig. 2. Quantitative, real-time DUB activity assays with a Ub sensor.

K48-linked Ub_5OM(LY) (10 nM), a mimic of a polyubiquitinated protein conjugate, was mixed with 5 μM OTUB1 with or without 20 μM UbcH5c at 25 °C in the presence of 2 nM Atto532-tIVR, and Atto532-tIVR fluorescence was monitored (left panel). A standard (STD) curve of Atto532-tIVR titrated with Ub (see Supplementary Fig. S5e) was used to convert the fluorescence intensity of Atto532-tIVR to free Ub concentration (right panel).

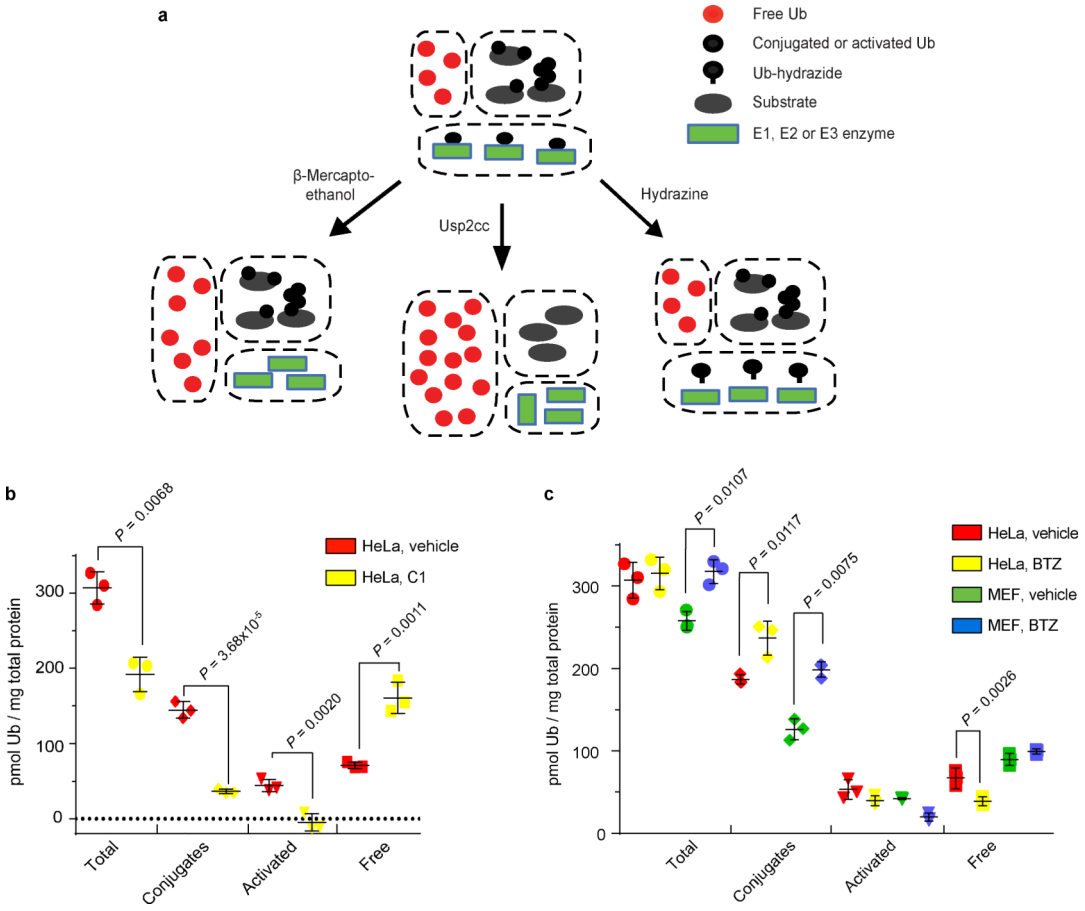

Fig. 3. Effects of cellular stresses on Ub pools.

a, Scheme used for the in-solution Ub pool measurements. **b,c**, Quantitation of Ub pools in lysates of indicated cell lines after treatment with vehicle (DMSO) or (**b**) E1 inhibitor, C1, at 10 μM or (**c**) proteasome inhibitor, BTZ, at 1 μM for 1 h. Statistical analyses by t-test (**b**) and ONE-WAY ANOVA with Bonferroni's adjustment (**c**); error bars represent ± s.d. (n = 3).

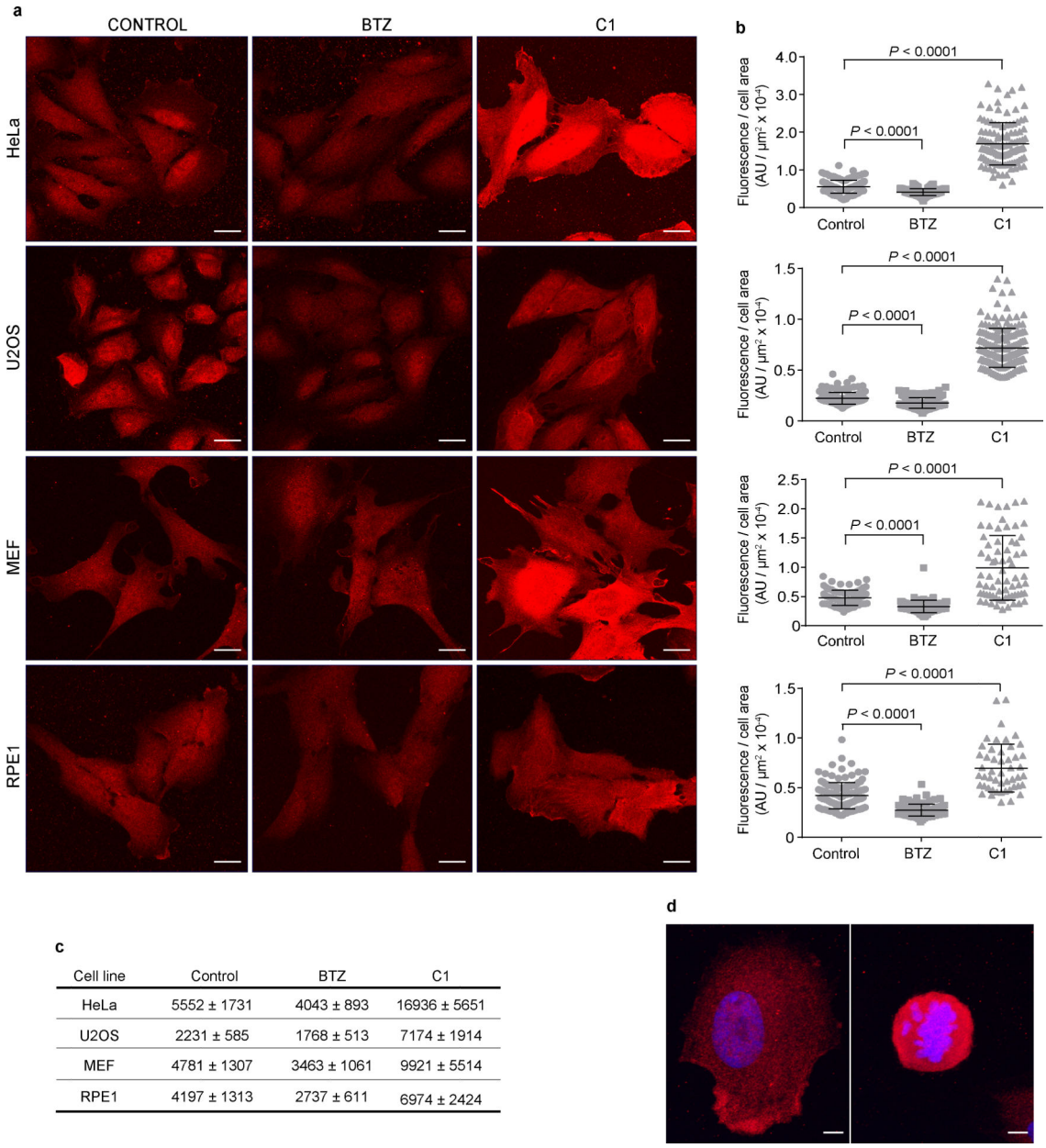

Cell line	Control	BTZ	C1
HeLa	5552 ± 1731	4043 ± 893	16936 ± 5651
U2OS	2231 ± 585	1768 ± 513	7174 ± 1914
MEF	4781 ± 1307	3463 ± 1061	9921 ± 5514
RPE1	4197 ± 1313	2737 ± 611	6974 ± 2424

Fig. 4. Free Ub staining in fixed and permeabilized HeLa, U2OS, MEF and RPE1 cells.

a, Maximum projection images of free Ub staining with HA-tUI in HeLa, U2OS, MEF and RPE1 cells after 1 h incubation with 1 μM proteasome inhibitor, BTZ or 10 μM E1 inhibitor, C1. Scale bars, 20 μm. **b**, Mean fluorescence for HeLa, U2OS, MEF, and RPE1 cells after 1 h incubation with 1 μM proteasome inhibitor or 10 μM E1 inhibitor. AU, arbitrary units. Cells analyzed per condition: HeLa, control n = 131, BTZ n = 125, C1 n = 116; U2OS, control n = 161, BTZ n = 170, C1 n = 175; MEF, control n = 80, BTZ n = 79, C1 n = 69; RPE1, control n = 133, BTZ n = 87, C1 n = 49. Bars show mean ± s.d. Statistical analyses used two-tailed unpaired Student's *t*-test with Welch's correction where appropriate. **c,** Relative free Ub from staining (mean fluorescence ± s.d.) of untreated cells or after proteasome or E1 inhibition. **d,** Representative interphase (left panel) and mitotic (right

panel) RPE-1 cells stained with HA-tUI (red) and DAPI (blue). Intensity measurements from 3D reconstructions employed Imaris software. Total cell fluorescence (arbitrary units; mean ± s.d.) for interphase and mitotic RPE1 cells were 23.7 ± 2.5 (n = 5) and 38.4 ± 3.5 (n = 3), respectively, whereas fluorescence per unit volume was 134.1 ± 8.6 for interphase cells and 463.2 ± 70.6 for mitotic cells. Scale bars, 5 μm.